Transient Anisotropy and Fragment Rotational Excitation in the Femtosecond Photodissociation of Triiodide in Solution

Thomas Kühne and Peter Vöhringer*

Abteilung Spektroskopie und Photochemische Kinetik, Max-Planck-Institut für Biophysikalische Chemie, Am Fassberg, D-37077 Göttingen, Germany, and Institut für Physikalische Chemie und Elektrochemie, Universität Karlsruhe, Kaiserstrasse 12, D-76128 Karlsruhe, Germany

Received: September 29, 1997; In Final Form: November 14, 1997

Transient anisotropy experiments on the triiodide photodissociation reaction in liquid solution are presented for excitation with 30-fs, 400-nm optical pulses. The decay of the spatial diatomic fragment distribution that is initially created through the process of bond fission occurs on three distinct time scales. On an ultrashort time scale well below 1 ps, an inertial contribution can clearly be distinguished. The corresponding Gaussian decay is described by correlation times around 450 fs. This ultrafast component reflects substantial rotational excitation of the diatomic product which results from impulsive photodissociation of the parent molecule. The contribution of the bending coordinate to the reaction mechanism in liquid solution is emphasized using a simple impulsive model for rotational excitation of the diatomic fragment. An intermediate time scale is characterized by an additional exponential contribution to the anisotropy decay with time constants around 2 ps and coincides with the time scale for vibrational relaxation of the diatomic fragment. On even longer times scales, rotational diffusion of the diatomic fragment governs the anisotropy decay with typical time constants of about 12 ps. A pronounced probe wavelength dependence of the rotational diffusion time constant is explained by an effective hydrodynamic volume that is detected by the probe pulse and originates from the anharmonicity of the diiodide potential. Finally, nuclear coherences at the diiodide vibrational frequency are observed in the inertial decay of the anisotropy. This novel effect is speculated to arise from a coupled motion of the system along all possible bending and stretching coordinates.

I. Introduction

Understanding the mechanisms and time scales of chemical reactions is one of the most intriguing issues in condensed-phase dynamics. Photoinduced fragmentations of triatomic molecules into atoms and diatoms are compelling model systems for the study of various elementary steps that generally compose a chemical transformation.[1]

For certain cases, these reactions can be initiated with an ultrashort light pulse such that the subsequent inherent molecular dynamics are virtually decoupled from the initial act of photon absorption.[2−8] The resulting coherent response of the system reflects motion along the reaction coordinate toward the product region. Dynamics in the vicinity of the transition state of the corresponding bimolecular full collision can be monitored, and the time scale for the fundamental reactive event can be characterized with high accuracy.[2,9−11] Furthermore, by studying the fragments in their so-called asymptotic limit, scalar properties of the reaction such as electronic and vibrational product state distributions can be exposed.[3,4,6−8,12−16] Interactions of the reactive system with the dense environment leads to damping and/or dephasing of coherent nuclear motion along the reaction coordinate as well as to dissipation of excess energy that is stored in fragment degrees of freedom.[15]

Furthermore, femtosecond experiments combined with polarization control of the optical radiation fields can be used in order to access vectorial properties associated with the chemical transformation. The key observable in these kinds of experiments is the transient optical anisotropy of the system, which is related to the second Legendre polynomial of a two-time dipole correlation function.[17] Important insight can be gained about the relative alignment of reactants, transition states, and products.[2,18,19] Polarization sensitivity can also help unravel symmetry properties[20,21] of the electronic potential energy surfaces relevant for breaking of the bond. Thus, valuable information is obtained about electronic correlations that facilitate the interconversion of reactants and product molecules.

Time-resolved polarization experiments have mostly been carried out in order to explore the dynamics of molecular rotational motion in liquid solution.[17] The transient optical anisotropy provides the necessary link to frequency-domain techniques such as Raman and Rayleigh-wing scattering or nuclear magnetic resonance.[22,23] From both theoretical and experimental studies it is now evident that molecular rotational motion in condensed media resembles the free-rotor dynamics on ultrashort time scales ($t < 10^{-12}$ s) and the Brownian-rotor dynamics on longer time scales ($t > 10^{-12}$ s).[22−27] This behavior is theoretically well-captured by extended diffusion models originally introduced by Gordon.[25−27]

This time-scale separation implies that it should be possible to investigate rotational excitation and reorientational dynamics of a diatom that results from impulsive photodissociation of a triatomic parent molecule. Provided the reaction is essentially complete before rotational excess energy can be dissipated into the surrounding liquid, such studies can reveal important information about initial rotational product state distributions that is otherwise not available in reactive condensed-phase systems. In addition, solvent-induced randomization of the

* To whom correspondence should be addressed.

S1089-5639(97)03154-X CCC: $15.00
Published on Web 01/15/1998

angular distribution of the photoproducts can be explored, which is connected to the correlation function of the fluctuating torques imparted to the system by the surrounding solvent cage. These dynamics may be intimately related to the processes of vibrational and rotational energy relaxation.

This paper presents femtosecond time-resolved anisotropy measurements on the 400-nm photodissociation reaction of triiodide in liquid ethanol solution. This reaction has been studied in great detail by Ruhman and co-workers using femtosecond optical pulses at 308 nm.[3,4,6,12−14,28−30] They could show that diiodide ions are formed within 400 fs after impulsive optical excitation. The diatomic product was shown to vibrate coherently, which indicates that the reaction is faster than solvent-induced dephasing of the nuclear coherence initially created by the photolysis pulse. We have recently uncovered dynamics of the same reaction initiated with 266-nm, 30-fs optical pulses which originate from the transition-state region of the bimolecular I_2^-/I encounter.[15,31] Wavelength-selective probing was employed in order to span detection windows along the nominal reaction coordinate through which the impulsively prepared wave packet will pass at characteristic delays after photoexcitation. Furthermore, information about the vibrational product state distribution has been obtained through transient resonance impulsive stimulated scattering[13] as well as through instantaneous absorption spectra of the diatomic product.[15] Additional information comes from resonance and preresonance light scattering experiments conducted by Myers and co-workers, which identify the symmetric stretching coordinate as the dominant contribution to the reaction coordinate at early times.[32−34] Furthermore, those studies show that solvent-induced symmetry breaking plays an important role in determining the degree of coherence that can be observed in the newly created fragments.[30,32−34]

The experiments reported here are closely related to most recent experiments performed by Hochstrasser and co-workers on the photodissociation reaction of mercury diiodide in ethanol solution.[35] The pump−probe anisotropy data reveal reactive motion from the initially prepared Franck−Condon region of HgI_2 toward the product region with HgI and I. The subsequent decay of the anisotropy was shown to occur in a biphasic manner containing an inertial component at early times below 1 ps and a slower diffusive component with a time constant of several picoseconds. As evidenced by supplementary equilibrium molecular dynamics simulations of HgI, the dynamics of rotational energy relaxation were shown to be extremely fast.[35]

The paper is organized as follows. Some details relevant to anisotropy measurements will be presented in section II together with a brief overview of the laser system that was used for the experiments reported here. Section III summarizes the experimental results obtained for the photodissociation of triiodide induced with 400-nm excitation light. The data will be discussed in section IV in terms of the multiple time scales that are observed in the transient optical anisotropy decay. Finally, a summary of the major results is presented in section V.

II. Experimental Section

Anisotropy experiments have been carried out with an entirely home-built laser system described elsewhere.[15] Briefly, 15-fs, 800-nm optical pulses from a Kerr lens mode-locked Ti:Sapphire laser were temporally broadened by a factor of 1000 in a diffractive pulse stretcher. Subsequent amplification in a regenerative amplifier yielded pulse energies as high as 1 mJ with a repetition rate of 1 kHz. Pulse compression in a standard

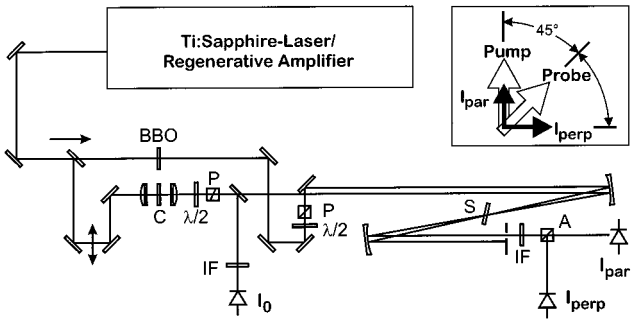

Figure 1. Schematic of the experimental setup. C: continuum generation. P: polarizer. IF: interference filter. A: analyzing polarizer. S: sample cell. The inset illustrates the polarization conditions used for the anisotropy experiments.

double-pass grating arrangement yielded pulse durations of approximately 30 fs with an overall throughput of about 50%. Photolysis pulses at 400 nm were obtained by frequency doubling the amplified pulses in a 100-μm-thick type-I BBO crystal with an efficiency of approximately 10%. The pulse duration of the second-harmonic pulses was also 30 fs, as determined through noncollinear difference frequency mixing with the fundamental in a 100-μm-thick type-I BBO crystal. To obtain probe pulses tunable in the visible/near-infrared spectral region, less than 1 μJ of the fundamental pulses was focused into a sapphire substrate with a thickness of 1 mm. Owing to its Gaussian beam profile and its excellent pulse-to-pulse stability, the emerging white-light continuum was used without additional parametric amplification. Anisotropy experiments were carried out in the pump−probe arrangement shown schematically in Figure 1. The relative pump and probe polarizations were set at 45° using zero-order half-wave retardation plates (mica, K. Lambrecht) and Glan-Taylor polarizers (K. Lambrecht). Both pulses were temporally and spatially overlapped in the sample using all-reflective optics with a radius of curvature of 1 m. Wavelength selection with a resolution of approximately 10 nm was achieved by using interference filters placed in the probe beam path behind the sample. A Wollaston prism polarizer (Spindler and Hoyer) behind the sample was used to separate those components of the probe light which were polarized parallel and perpendicular with respect to the *E*-field vector of the pump pulse. For each laser shot, the intensities I_{par} and I_{perp} of both components were detected simultaneously together with the reference intensity I_0 of the probe light in front of the sample. The transient anisotropy at pump−probe time delay τ was calculated from successive laser shots according to

$$r(\tau) = \frac{\Delta OD_{par}(\tau) - \Delta OD_{perp}(\tau)}{\Delta OD_{par}(\tau) + 2\Delta OD_{perp}(\tau)} \quad (1)$$

Here, $\Delta OD_{par,perp}$ denotes the pump-induced optical density detected parallel/perpendicular with respect to the pump pulse polarization:

$$\Delta OD_{par,perp}(\tau) = \log\left(\frac{I_0(\tau)}{I_{par,perp}(\tau)}\right) - \log\left(\frac{I_0(\tau)}{I_{par,perp}(\tau)}\right)_W \quad (2)$$

The index W indicates a measurement of the optical density in the absence of the pump pulse. The simultaneous detection of the parallel and perpendicular components of the optical density has the great advantage that shot-to-shot fluctuations automatically cancel in eq 1. This is not the case if $r(\tau)$ is calculated from independent scans of the parallel and perpendicular

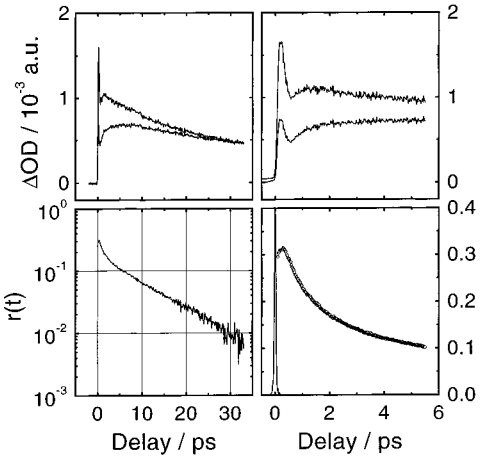

Figure 2. Experimental pump−probe transient and calculated anisotropy at a probe wavelength of 800 nm. Left column: long-time behavior. Right column: short-time behavior and experimental instrument response function.

components of the pump-induced optical density (e.g., through rotation of the probe pulse polarization in front of the sample). Furthermore, no balancing of the parallel and perpendicular signal intensities is required as $r(t)$ is calculated directly from pump-induced optical densities (see eq 2). Pump-pulse energies were always kept well below 1 μJ to avoid saturation effects. Saturation was tested for by monitoring the maximum anisotropy while continuously decreasing the excitation density until the pump-induced optical density completely disappeared. An initial anisotropy of 0.4 could be recovered for triiodide excited and probed at degenerate wavelengths of 400 nm. The overall time resolution in this detection scheme was always well below 70 fs throughout the entire wavelength range covered by the white-light continuum (see also Figures 2−4). The instrument response was much shorter than all the dynamics to be discussed in this paper. Triiodide solutions in ethanol with a concentration of 3 mM were prepared according to ref 15. All chemicals were obtained from Aldrich and were used without further purification.

III. Results

Figures 2−4 show representative probe wavelength resolved parallel and perpendicular transients of triiodide solutions in ethanol following 400-nm excitation. Also displayed are the resulting transient anisotropies on a semilogarithmic scale. The experimental $r(t)$ values exhibit an excellent signal-to-noise ratio with a dynamic range of almost 3 orders of magnitude. The high quality of the data results from the simultaneous detection scheme described in the previous section. The short-time optical responses together with the corresponding anisotropies are also displayed in Figures 2−4.

It is obvious that at all probe wavelengths the anisotropy decays in a highly nonexponential fashion. However, the analysis of these data is very straightforward, as demonstrated in Figure 5 for a probe wavelength of 730 nm. First, the long-time tail of $r(\tau)$ is manually fitted to an exponential (cf. Figure 5a). The resulting residuals clearly expose an additional exponential component to the anisotropy whose amplitude and time constant can also be determined manually (Figure 5b). Again, the residuals are calculated, which uncover a final Gaussian component on a time scale well below 1 ps, the amplitude and correlation time of which are also manually estimated as shown in Figure 5c. Finally, the total anisotropy

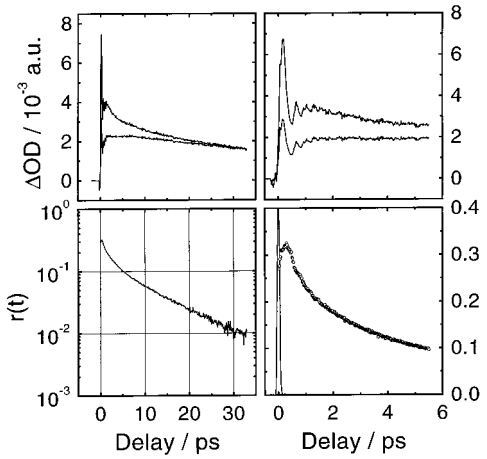

Figure 3. Experimental pump−probe transients and calculated anisotropies at a probe wavelength of 700 nm.

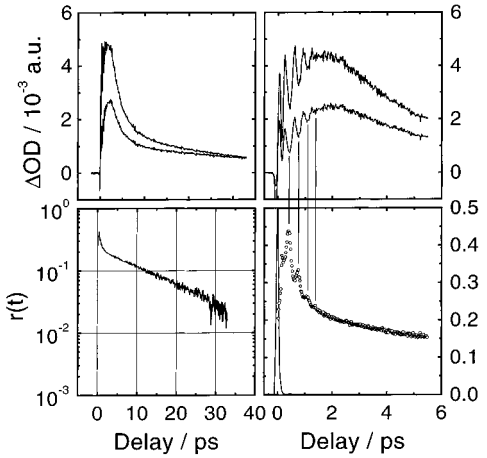

Figure 4. Experimental pump−probe transients and calculated anisotropies at a probe wavelength of 530 nm.

is modeled according to

$$r(\tau) = A_1 \exp\left(-\frac{\tau}{\Gamma_1}\right) + A_2 \exp\left(-\frac{\tau}{\Gamma_2}\right) + A_3 \exp\left(-\left(\frac{\tau}{\Gamma_3}\right)^2\right) \quad (3)$$

using a Levenberg−Marquardt routine with the predetermined fit parameters as an initial guess for the set of amplitudes A_i and time constants Γ_i appearing in eq 3. The resulting fit parameters are summarized in Table 1. It should be pointed out here that this method of fitting is not strictly correct because the proper convolution of the parallel and perpendicular signals with the finite instrument response is neglected. However, Figures 2−4 demonstrate that such a convolution is not required since the time scale of even the fastest contribution to $r(t)$ is well above the experimental time resolution.

The time constant for the slowest exponential decay clearly increases as the probe pulse is tuned from the red to the blue. Simultaneously, the corresponding amplitude behaves nonmonotonically, having a minimum around 680 nm. In parallel, the time constant for the fast exponential component seems to exhibit a maximum at this wavelength. However, the scatter in the experimental data is too large to draw definite conclusions. The correlation time and amplitude of the Gaussian component is relatively wavelength independent with an average value of 0.45 ps.

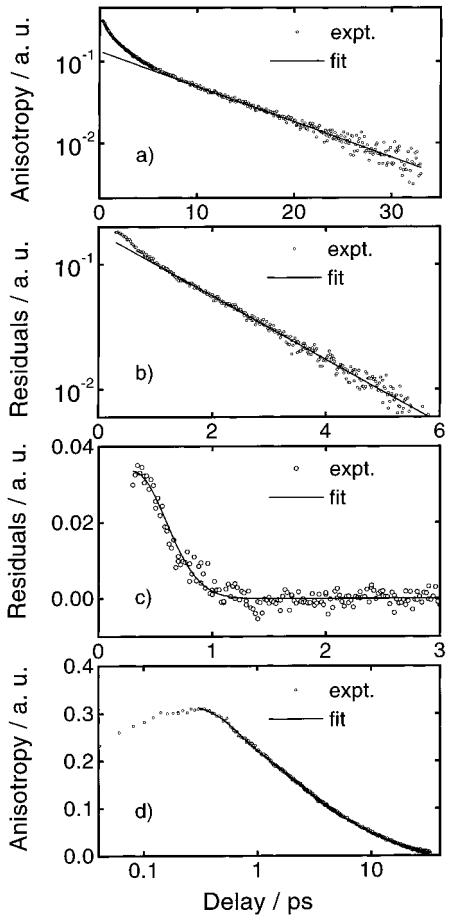

Figure 5. Analysis of the transient anisotropy data at a probe wavelength of 730 nm. Open circles: experimental data. Solid lines: exponential fit. (a) Raw data; (b) residuals calculated from (a) and exponential fit; (c) inertial component obtained from (a) and (b); (d) global nonlinear least squares using eq 3.

TABLE 1: Fit Parameters Obtained from a Nonlinear Least-Squares Fit of the Anisotropy Data to Eq 3

λ_{probe}/nm	A_1	Γ_1/ps	A_2	Γ_2/ps	A_3	Γ_3
800	0.161	10.7	0.126	1.23	0.021	0.46
730	0.129	11.1	0.150	1.71	0.034	0.41
700	0.129	11.9	0.146	2.12	0.045	0.42
680	0.085	12.7	0.155	2.65	0.041	0.45
650	0.117	12.8	0.128	2.48	0.053	0.66
630	0.154	12.7	0.094	1.91	0.050	0.48
610	0.137	13.2	0.087	2.56	0.065	0.70
550	0.220	14.5				
530	0.215	15.7	0.132	0.70	0.080	0.47

These data will be discussed in the following section in terms of the various dynamic processes involved in the triiodide photodissociation.

IV. Discussion

Prior to a discussion of the time-dependent anisotropy, a brief overview of the pump-induced optical density is given to orient the reader. At early times, the signal exhibits a sharp spike, which stems from transient absorptions of the Franck−Condon regions as well as the transition-state region of the bimolecular iodine−diiodide full collision. A more comprehensive treatment of this feature including its probe wavelength dependence is given in ref 31. The earliest delay at which diiodide product ions can be identified unambiguously is around 350 fs. Here, a pronounced shoulder can be detected close to the minimum of the pump-induced transient absorption. Interestingly, for most probe wavelengths, the time-dependent anisotropy reaches a maximum value at this particular delay. The subsequent rise of the transient absorption which lasts for about two vibrational periods of the diatomic product corresponds to the full collapse of the wave packet into the exit channel, the subsequent recoil of the fragments, and the onset of vibrational thermalization. It is here where the anisotropy displays its Gaussian decay. The complicated interplay of all these aspects of the triiodide photochemistry is not yet fully understood. At certain wavelengths, for instance, a clear bump at delays around 7 ps can be observed, which is associated with vibrational cooling near the bottom of the diiodide well. A complete picture of the dynamics of vibrational relaxation uncontaminated by the process of geminate recombination can be obtained only from longer delays through reconstruction of instantaneous absorption spectra of the diatomic product.[15,36]

A. Inertial Dynamics. It was shown in section III that the initial decay of the anisotropy resembles a Gaussian with a correlation time of about 0.45 ps. The anisotropy measures the correlation function of the second Legendre polynomial of the scalar product of pump and probe transition dipoles.[17]

$$r(\tau) = \frac{1}{5}\langle P_2[\mu_{\text{Pump}}(0)\mu_{\text{Probe}}(\tau)]\rangle = \frac{2}{5}\langle P_2[\cos\theta]\rangle \qquad (4)$$

Here, θ is the angle between the transition dipole of the pump transition at time delay $\tau = 0$ and that of the probe transition at time delay τ. In the case of a dissociation reaction[10,11,18,19] with the probe pulse being sensitive to the product, θ denotes the angle between the reactant dipole at $\tau = 0$ and the product dipole at time delay τ. For the moment, both dipoles are assumed to be oriented parallel to the bond axis of the diatomic fragment.

For an ensemble of free diatomic rotors at temperature T, eq 4 can be solved numerically from a Maxwell distribution, $P(\omega_0)$, of rotational velocities, ω_0:[22]

$$r(t) = \frac{2}{5}\left[\frac{1}{4} + \frac{3}{4}\int_0^\infty \mathrm{d}\omega_0\, P(\omega_0)\cos(2\omega_0 t)\right] \qquad (5)$$

In an equilibrium canonical ensemble, $P(\omega_0)$ is given by

$$P(\omega_0) = \left(\frac{I}{k_B T}\right)\omega_0 \exp\left(-\frac{I\omega_0^2}{2k_B T}\right) \qquad (6)$$

where k_B denotes the Boltzmann constant and I is the moment of inertia of the diatom (1.1×10^{-44} kg m^2 for I_2^- calculated at its equilibrium position). The initial part of the anisotropy decays as a Gaussian with the free-rotor orientational correlation time $\tau_c = (I/3k_B T)^{1/2}$.

$$r(t \to 0) \approx \frac{2}{5}\exp\left[-\left(\frac{t}{\tau_c}\right)^2\right] \qquad (7)$$

For diiodide ions at room temperature, the value for τ_c is 0.95 ps. Assuming the dissociation reaction occurs instantaneously and generates diatomic fragments in a Boltzmann distribution of rotational velocities at temperature T, eqs 5−7 describe the temporal behavior of the anisotropy provided the process is carried out under isolated molecule conditions. As the environment becomes more dense approaching liquid-phase densities, collisions should affect the temporal behavior of $r(\tau)$ until the diffusion limit with a pure exponential decay is attained. However, at early times the decay of the correlation function remains inertial and is determined only by the temperature and the moment of inertia of the system. This is also reflected to

a significant extent in Raman line shapes of diatomic molecules in condensed-phase environments.[25−27,37−39] Following Gordon, the short-time behavior of the anisotropy can be expressed as a time-series expansion.[25−27]

$$r(t) = \frac{2}{5}\left\{1 - \left(\frac{3k_BT}{I}\right)t^2 + \left[\left(\frac{2k_BT}{I}\right)^2 + \left(\frac{\langle Q^2\rangle}{8I^2}\right)\right]t^4 \ldots\right\} \quad (8)$$

where $\langle Q^2\rangle$ is the mean-square torque imparted to the molecule by other neighboring molecules. The initial curvature of the correlation function resembles the motion of freely rotating molecules at temperature T, as given by eq 7. However, the effect of intermolecular forces is to slow the decay of $r(\tau)$ by the fourth power of t.

Assuming the photodissociation reaction of triiodide generates a Boltzmann-like distribution, the inertial component to the anisotropy shown in Figure 5 is a direct measure of the rotational temperature of the diatomic fragments. The average experimentally observed correlation time τ_c is 450 fs. Thus, a rotational temperature of 1300 K of the nascent diiodide photofragments can be estimated, which by equipartitioning corresponds to a mean rotational energy of about 1000 cm^{-1}. The average bond length of diiodide at early times may deviate significantly from its equilibrium value of 2.95 Å. Since the rotational correlation time scales with the square root of the moment of inertia and, thus, directly with the internuclear distance, a rotational temperature of 300 K would be consistent with $\tau_c = 450$ fs only if the diodide bond is compressed by an unreasonable factor of $\sqrt{1300}/\sqrt{300} \approx 2$. Therefore, we can conclude that a significant amount of excess energy provided by the 400-nm photon is deposited into the rotational degrees of freedom of the fragments.

Provided that the initial ultrafast component of the anisotropy indeed arises from free-streaming rotational motion of the diiodide fragments, eq 5 can also be solved for product rotational distributions other than those given by eq 6. As was shown by Baskin and Zewail for isolated molecule conditions,[19] the anisotropy decay remains Gaussian if the photodissociation generates a Gaussian distribution centered at a rotational quantum number of $j = 0$ with a half-width at $1/e$ of Δj.

$$r(t) = \frac{2}{5}\left\{\frac{1}{4} + \frac{3}{4}\exp\left[-\left(\Delta j\frac{I}{\hbar}\right)^2\right]\right\} \quad (9)$$

By comparison with the experimentally determined correlation time τ_c, one obtains a value for Δj of 230. The mean rotational energy $\langle E_{rot}\rangle = \sum_j [Bj(j+1)P(j)]$, where $B = h/(8\pi^2 cI)$ is the rotational constant in cm^{-1}, amounts to approximately 700 cm^{-1}. This is again much higher than the value of 200 cm^{-1} expected for a room-temperature ensemble. The corresponding distribution function $P(j) = (2/\Delta j\sqrt{\pi})\exp(-j^2/\Delta j^2)$ is reproduced in Figure 6. For comparison, the one-dimensional Boltzmann distribution $P(j, T{=}1300\text{K}) = 2j\exp[-hcBj^2/(k_BT)]$ obtained from the previous fit is also displayed.

Finally, eq 5 can also be solved for a Gaussian distribution with a nonzero central quantum number j_0 with the constraint $j_0 \gg \Delta j$. In this case, however, the anisotropy follows a damped oscillation.[19]

$$r(t) = \frac{2}{5}\left\{\frac{1}{4} + \frac{3}{4}\cos\left(2j_0\frac{I}{\hbar}\right)\exp\left[-\left(\Delta j\frac{I}{\hbar}t\right)^2\right]\right\} \quad (10)$$

The initial decay is determined by the central quantum number of the rotational product distribution. The width of $P(j)$ gives rise to loss of rotational coherence and to damping of the anisotropy oscillating at the most probable rotational period $\omega = 4\pi Bj_0$ of the ensemble. As demonstrated by Baskin and Zewail for the photodissociation of HgI_2 under isolated molecule conditions,[19] the amplitude and temporal position of a dip discernible after the initial decay of $r(t)$ gives direct and immediate information about the product-state distribution of the fragments. In the anisotropy experiments reported here for the photodissociation reaction of diiodide in liquid solution no such dip was detected. This indicates that solvent-induced randomization of the diiodide orientational distribution is more important than coherence decay that results from the finite width of the rotational-state distribution.

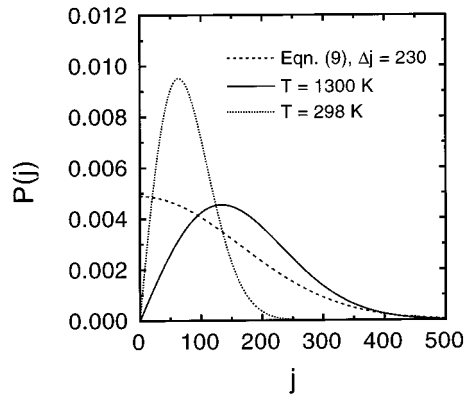

Figure 6. Rotational distribution functions of the diiodide fragment. Solid: Boltzmann distribution at a rotational temperature of 1300 K. Dashed: Gaussian distribution obtained from eq 9. Dot−dashed: room-temperature Boltzmann distribution.

For the sake of completeness, however, we fitted the Gaussian component of the experimental anisotropy to eq 10 again assuming that the ultrafast decay corresponds to motion of a collection of free noninteracting rotors. The resulting central quantum number is around $j_0 = 140$, consistent with the Boltzmann distribution at a rotational temperature of 1300 K (see Figure 6). Again, this gives direct evidence for a significant rotational excitation of the products. However, the width of the distribution has to be set to $\Delta j = 170$ in order to be consistent with a mean rotational excitation of about 1000 cm^{-1}. Thus, $\Delta j > j_0$, and as mentioned by Baskin and Zewail, eq 10 does not provide a good approximation for the anisotropy decay.[19]

In any case, the inertial contribution to the anisotropy reveals substantial rotational excitation of diiodide ions generated through impulsive 400-nm photodissociation of triiodide in ethanol solution.

B. Initial Anisotropy. For pump and probe transition dipoles oriented parallel with respect to each other, eq 4 predicts a value for the initial anisotropy at $\tau = 0$ of 0.4. This is also the value one would expect for a photodissociation reaction of a linear triatomic molecule if both transition dipoles are oriented parallel to the bond axis of the diatomic fragment. Triiodide ions in liquid solution have two strong absorption bands in the UV/near-UV spectral regions centered at 360 and 280 nm, respectively. Both dissociative resonances are known to have transition dipoles polarized along the long axis of the molecule.[40−42] Diiodide product ions have strong absorptions around 400 and 800 nm. The latter near-IR resonance corresponds to a $\Pi \leftarrow \sum$ transition with the transition dipole oriented along the molecular bond.[43] Hence, provided triiodide assumes a linear geometry in solution, an anisotropy of 0.4 is expected. We will come back to this point later in this section.

In the previous section, it was shown that bond fission initiated at 400 nm results in significant rotational excitation of

the diiodide product. Fragment rotational excitation can arise from three different sources. First, overall rotational excitation of the ground-state parent molecule (before impulsive excitation has taken place) results in an increase of the total angular momentum of the fragments. Second, excitation of the bending vibration of the ground-state parent molecule translates into rotational excitation of the diatomic product after the process of bond fission is complete. Since motion along the bending coordinate essentially corresponds to a hindered rotation of the future diatomic fragment, bending excitation translates into rotational motion of the diatomic product about its center-of-mass. Finally, possible anisotropies in the dissociative potential energy surface can generate torques on the diatom that is recoiling from the monatomic fragment. In this case, the final rotational-state distribution mainly reflects the topology of the upper excited electronic state of the parent molecule.

No detailed information about the excited electronic surfaces of triiodide along the bending angle is available. There exists an empirical LEPS potential for the linear encounter of diiodide ions with iodine radicals that has been optimized by fitting an experimental absorption spectrum using classical MD simulations.[12] This potential, however, is not useful to estimate the rotational excitation of the I_2^- fragment. Therefore, the data are interpreted using the so-called impulsive model for rotational excitation.[44−46] Within this model, the diiodide bond is assumed to be infinitely stiff such that vibrational excitation of the diatomic fragment is negligible. The repulsive force between the center and the outer iodine atom results in rotation of the diatom about its center-of-mass if the configuration of the parent molecule is instantaneously bent at the moment of bond fission (symmetry C_{2v}). Following Levene and Valentini, one obtains by energy and angular momentum conservation[45]

$$E_{\mathrm{ROT}} = E_{\mathrm{EXC}} \frac{\sin^2 \alpha}{4 - \cos^2 \alpha} \tag{11}$$

where E_{EXC} denotes the excess energy provided by the laser pulse with respect to the electronic energy of the well-separated fragments. If the parent molecule already exhibits a nonvanishing bend angle at its equilibrium geometry, eq 11 gives immediate access to the center quantum number of the rotational product distribution. If, on the other hand, the mean rotational energy is known, one can obtain the equilibrium geometry along the bending coordinate. Using an excess energy of 1.2 eV provided by the 400-nm pump pulse and a mean rotational energy of approximately 1000 cm^{-1} as estimated from the inertial contribution to the anisotropy, a bend angle of 146° is obtained. Therefore, the angle spanned by the pump and probe transition dipole is 17° provided the pump transition dipole is oriented along the long axis of the molecule. According to eq 4, one would expect an initial anisotropy of 0.35. The average maximum anisotropy observed in the current experiments is 0.33, in good agreement with these simple model calculations.

However, eq 11 has to be weighted by the actual distribution of bending angles of the parent molecules in order to obtain the rotational-state distribution of the diatomic fragment. To do so, information about the bending vibration of ground-state triiodide is necessary. From IR spectra of triiodide in nitrobenzene solution the bending vibration is known to have a vibrational frequency of 70 cm^{-1}.[47] The total harmonic oscillator probability distribution of ground-state triiodide as a function of bending angle θ is shown in Figure 7 for a temperature of 298 K. Again, an equilibrium bend angle of 146° was assumed. The resulting rotational distribution function

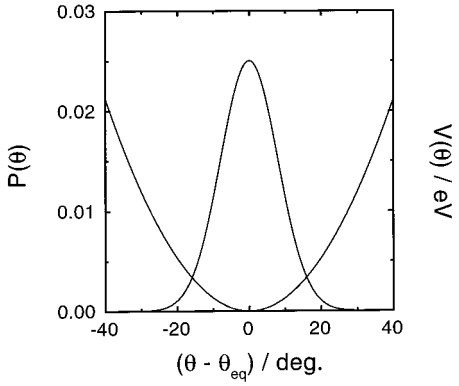

Figure 7. Room-temperature equilibrium distribution of the diiodide bending harmonic oscillator.

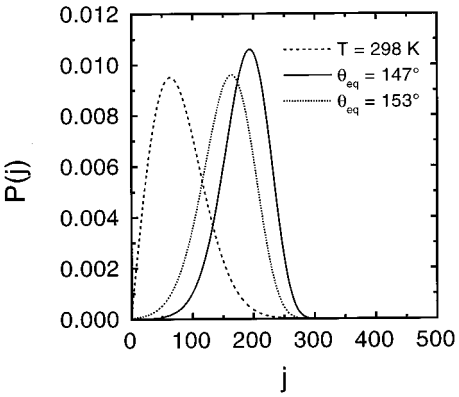

Figure 8. Rotational distribution function obtained from the impulse model for rotational excitation. Solid: equilibrium bend angle of 147°. Dotted: equilibrium bend angle of 147°. Dashed: room-temperature Boltzmann distribution

is displayed in Figure 8 as the solid curve. For comparison, the room-temperature Boltzmann distribution is also shown as the dashed curve. $P(j)$ peaks around $j = 200$ and has a full width at $1/e$ of approximately $\Delta j = 100$. It closely resembles a distribution function that would give rise to an anisotropy decay given by eq 10. As was pointed out in the previous section, solvent-induced randomization of the I_2^- orientational distribution takes over before the predicted characteristic dip in $r(\tau)$ can appear. However, using a Gaussian distribution centered at $j = 200$ with a $1/e$ width of $\Delta j = 100$, the calculated $r(t)$ cannot reproduce the initial curvature of the experimental data. A bend angle of 153° gives rise to a distribution centered at $j = 165$ with a width at $1/e$ of approximately 100 (dotted−dashed curve in Figure 8). The corresponding mean rotational energy has a value of 700 cm^{-1}, still consistent with an excitation as calculated from eq 9. Furthermore, the resulting $r(t)$ can now reproduce the initial curvature of the experimental data. Finally, the anisotropy at $t = 0$ is expected to have a value of 0.36, still in qualitative agreement with experiment.

It has to be mentioned here that triiodide ions are commonly believed to be linear in liquid solution. Resonance Raman studies conducted by Myers and co-workers, however, demonstrate that the symmetry is considerably broken in liquid solution. This is evidenced by a significant Raman activity of the antisymmetric stretching vibration.[32−34] This mode appears also in resonance impulse stimulated scattering data performed in our laboratory.[15] Although not directly comparable, both findings are similar to those obtained from X-ray diffraction experiments on CsI_3 crystals that show that the geometry of ground-state triiodide can deviate significantly from a linear configuration.[48] We also reiterate that the preceding discussion

is based on the assumption that the ground state is bent. It is also possible that the ground state is linear while the excited state has a minimum at some finite angle along the bending coordinate. However, such a treatment requires detailed information about the dissociative potential energy surface as a function of all internal coordinates.

Finally, it has to be pointed out that the experimental anisotropy does not reach its maximum value at $\tau = 0$. Especially for wavelengths in the near-IR, $r(t)$ builds up from initial values that can be significantly lower than 0.3. The anisotropy reaches its maximum during the ultrafast decay of the transient absorption that follows the narrow spike at early times. As shown recently by us,[31] this sharp feature in the pump-induced optical density is reminiscent of dynamics in the transition-state region of the I_2^-/I full collision. The first signature of the diiodide product ions can be observed around 300 fs as a small modulation superimposed on the falling edge of the narrow spike. At this delay, the wave packet collapses into the exit channel for two-body dissociation and the diiodide bond is compressed for the first time after impulsive excitation. This corresponds to the moment of bond breakage, and it is here where the anisotropy reaches its maximum value. The preceding induction period observed in the transient anisotropy coincides with the ultrafast motion of the wave packet along the symmetric stretching coordinate away from the initially prepared Franck−Condon region.[31]

C. Diffusive Dynamics. The analysis of the experimental data reveals two exponentially decaying contributions to the anisotropy $r(\tau)$. Diffusive reorientation of the transition dipole moments will take place on longer time scales and is connected with an exponential decay of $r(\tau)$,[17]

$$r(t) = \frac{2}{5}\exp(-6D_s t) = \frac{2}{5}\exp\left(-\frac{t}{\tau_s}\right) \qquad (12)$$

where τ_s is the rotational diffusion time constant of the equivalent-volume sphere. D_s is the rotational diffusion coefficient of the spherical rotor which can be calculated according to the familiar Stokes−Einstein−Debye expression $D_s = k_B T/(6V\eta)$, where V is the volume of the body and η is the viscosity of the solvent (stick hydrodynamics). For nonspherical rotors, such as I_3^- and I_2^-, D_s has to be replaced with the appropriate diagonal element of the diffusion tensor in the molecular coordinate system. For ellipsoids these can be derived from D_s in terms of the axial ratio ρ (see ref 17),

$$D = D_s \frac{3}{2}\frac{\rho[(2\rho^2 - 1)S - \rho]}{\rho^4 - 1} \qquad (13)$$

where S is given by

$$S = (\rho^2 - 1)^{-1/2}\ln[\rho + (\rho^2 - 1)^{1/2}] \qquad (14)$$

The species that appear on longer time scales are diiodide ions in their electronic ground state and ground-state triiodide ions generated through geminate recombination of the fragments. The I−I bond lengths are 3.23 and 2.9 Å for I_2^- and I_3^-, respectively. Thus, one obtains rotational diffusion time constants of 15 ps for diiodide ions and 36 ps for triiodide, respectively. From these values, one would immediately conclude that the slow component of the anisotropy decay is due to rotational diffusion of the diiodide product ions.

However, stick hydrodynamic boundary conditions have been applied successfully only to larger molecules in solution. In contrast, for small molecules in the liquid phase, the rotational correlation time constants are often found to be significantly shorter than predicted by eqs 12−14.[17] Hu and Zwanzig derived a correction factor for so-called slip boundary conditions in terms of the axial ratio of the rotating body.[49] The diffusion coefficient can be approximated for $0 > \rho > 0.9$ by the empirical fit function

$$D_{slip} = D_{stick}\, A\left(1 - \frac{1}{\rho}\right)^{\alpha}\exp\left[-\left(\frac{1}{B\rho}\right)^{\beta}\right] \qquad (15)$$

where the coefficients are given by $A = 0.9134$, $B = 0.6536$, $\alpha = 1.12$, and $\beta = 2.15$. Using eq 15, rotational diffusion time constants of 3.7 ps for diiodide and 17 ps for triiodide are found. These numbers suggest that the diffusive biexponential decay on longer time scales reflects the rotational behavior of a mixture of species. The slow exponential component of $r(\tau)$ would be due to rotational diffusion of I_3^-, and the faster component would correspond to I_2^-. According to this interpretation, both reorientational dynamics would obey slip boundary conditions.

However, the absorption coefficient of vibrationally cold ground-state triiodide at 800 nm is essentially zero as compared to that of I_2^- (approximately 2500 M^{-1} cm^{-1}, see ref 50). Therefore, vibrationally excited rather than thermally equilibrated triiodide ions would have to be detected in the near-infrared. Furthermore, it was noticed that the time constant of the long-time exponential decay was probe wavelength dependent. As the probe pulse is tuned from the blue to the red, τ decreases by more than 50%. This behavior is shown in Table 1. If indeed vibrationally excited triiodide is detected on longer time scales, one would actually expect an opposite wavelength dependence. As the probe wavelength increases (i.e., tuned away from the UV resonances of I_3^-), the experiment becomes more sensitive to higher lying vibrational states of triiodide. Due to anharmonicities in the system, one can expect that a red probe wavelength would preferentially detect a more stretched configuration of triiodide unless geminate recombination creates ground-state triiodide in a highly bent configuration. Therefore, as the probe pulse is tuned further to the red, it becomes more sensitive to a larger effective hydrodynamic volume of the rotating triiodide ion. Besides, geminate recombination is expected to fully scramble the molecular orientations unless the solvent cage is highly isotropic and the process occurs to a certain extent coherently.

If, on the other hand, the rotating transition dipoles are associated with diiodide, the probe pulse becomes more sensitive to lower vibrational states as the wavelength is tuned into the I_2^- resonance. The probe pulse sensitivity to a given vibrational quantum state of diiodide is given by the spectral window function $P(\upsilon, \lambda)$ that we reported earlier.[15] The decreasing time constant with increasing probe wavelength can then be rationalized by the anharmonicity of the diiodide ground-state potential and the effective hydrodynamic volume detected by the probe pulse. The exponential time constant is plotted in Figure 9 as a function of the expectation value for the internuclear distance of diiodide. $\langle r\rangle$ was calculated from the Morse oscillator eigenfunction $|\upsilon\rangle$, to which the probe wavelength is most sensitive. Also shown in Figure 9 are the rotational diffusion time constants calculated for the ellipsoid with slip and stick hydrodynamic boundary conditions. The agreement between simulation and experimental data is not at all satisfactory. Slip boundary conditions underestimate the time constant by more than a factor of 2. Stick hydrodynamics overestimate the time constants, but the general trend can be recognized. This is due to a stronger ρ-dependence of eq 13 as compared to eq 15. Also shown in Figure 9 are the time constants of the equivalent

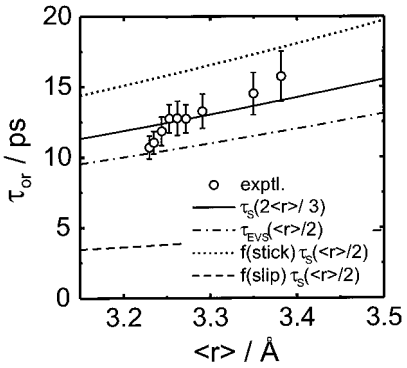

Figure 9. Rotational diffusion time constants as a function of mean internuclear separation of the diiodide oscillator. Short-dash: stick hydrodynamics. Long-dash: slip hydrodynamics. Dot−dash: equivalent-volume spherical rotor. Solid: equivalent-volume spherical rotor with radius $(2/3)\langle r\rangle$.

volume spheres with radii $\langle r\rangle/2$ and $3\langle r\rangle/2$, respectively. As opposed to the ellipsoid with the short semiaxis fixed, the volume of a sphere scales as $\langle r\rangle^3$. Therefore, the dependence of the rotational diffusion time constant on the internuclear separation is much more pronounced than in the case of slip hydrodynamics. The experimental data can be qualitatively reproduced, although the $\langle r\rangle$-dependence of the simulation is still somewhat too weak.

The qualitative agreement between the experimental data and the rotational correlation times of the spherical rotor is rather surprising. However, such a behavior has been observed before for some anionic dyes in alcohol solvents and was explained by solvent attachment. Hydrogen bonding smears out the molecular structure to form a near sphere with a diameter of approximately the largest molecular dimension.[51,52] By analogy, we conclude that strong hydrogen bonding between I_2^- and ethanol solvent molecules strongly affects the dynamics of rotational diffusion.

Finally, it should be mentioned that the frequency-dependent frictional response of the solvent may give a more adequate description of the diffusive reorientational dynamics. It is not at all clear whether the effective viscosity of ethanol in the first 10 ps after photodissociation of triiodide is identical to its steady-state value. A transient perturbation and local heating of the hydrogen-bonding network can be expected due to the impulsive recoil of the fragments. A full quantitative understanding of these effects must await more comprehensive theoretical treatments. Ethanol seems to be a rather rapidly responding liquid, as judged, for example, through time-resolved nonresonant Raman experiments (see ref 15). Nevertheless, the slowest nuclear contribution to the third-order Raman susceptibility of ethanol originates from rotational diffusion with a typical time constant around 8 ps. This is comparable to the time constant found for rotational diffusion of diiodide. The nature of the solvent modes that are able to restore the transiently disrupted hydrogen-bonding network as well as the time scale associated with these fluctuations still remain to be clarified.

E. Intermediate Dynamics. From earlier experiments conducted by Ruhman and co-workers[3] as well as from experiments performed in our laboratory,[13] it is clear that diiodide ions are initially formed with substantial excess vibrational energy. It was found that vibrational relaxation occurs very rapidly with a time constant of about 2−3 ps.[3,13] If the above interpretation of the wavelength dependence of $r(\tau)$ is correct, it may be that further separation of the fragments as well as vibrational cooling of the diatomic product leads to anisotropy decays that are highly nonexponential. This is because each probe wavelength is sensitive to specific molecular geometry of the diatomic fragment which randomizes with a characteristic rotational diffusion time. Provided the time scale for fragment separation and vibrational relaxation is well-separated from the time scale for rotational diffusion, the early portion of the anisotropy should also contain information about the dynamics of vibrational cooling and fragment separation rather than pure diffusive reorientation. Only in the asymptotic limit will the rotational diffusion time constant for an ensemble of diiodide rotors centered at the equilibrium distance be recovered. Indeed, the time constant of the fast exponential component is in qualitative agreement with the rate of vibrational relaxation.

Furthermore, it was shown in section IVA that the diiodide products are dressed with a significant amount of excess rotational energy. To our knowledge, dissipation of excess rotational energy in liquid solution has never been studied in a time-resolved experiment. Hochstrasser and co-workers have measured anisotropy decays of mercury iodide following photodissociation of HgI_2.[35] Their experimental data have been supplemented by equilibrium molecular dynamics simulations of the diatomic HgI in ethanol system. It was shown that the angular momentum correlation function and the rotational kinetic energy correlation function decay extremely rapidly, with time constants of 210 and 160 fs, respectively. Assuming linear response, this is the time required for relaxation of excess rotational energy.[35] By comparison, one is tempted to conclude that the fast exponential component observed here does not reflect the dynamics of rotational energy dissipation. Nevertheless, there is no direct evidence that these two systems have the same rotational energy relaxation time. The experiments presented here are not sufficient to explain the origin of the intermediate exponential relaxation of the time-dependent anisotropy. Further experiments are currently in progress in our group that focus specifically on this extremely important aspect of the triiodide photodissociation.

F. Nuclear Coherences. At certain probe wavelengths, modulations were observed in the residuals as well as in the raw anisotropy data whose frequencies agree precisely with the diiodide vibration. This behavior is illustrated in Figure 4 for a probe wavelength of 530 nm, where the modulation depth was largest. We point out that these modulations were only observed in the inertial region of the anisotropy decay. A wavelength of 530 nm spans a detection window at the inner turning point of the diiodide bond. The transient absorption exhibits a maximum whenever the diiodide bond is compressed. At the same time, the anisotropy exhibits a minimum which is visible for at least three vibrational periods. Complementary experiments on photodissociating HgI_2 performed by Volk et al. display a similar effect.[35] HgI vibrational coherences were observed in the time derivative of the anisotropy. As the wave packet oscillates between inner and outer turning point, the effective hydrodynamic volume changes accordingly. Since the rotational diffusion time is proportional to the hydrodynamic volume (see eq 12), wave packet motion results in a modulation of the rate for molecular reorientation at the oscillator frequency.[35] In the experiments reported here, coherences are not only observed in the instantaneous slope of $r(t)$. They are also detected directly in the anisotropy, indicating that not only the rate of molecular reorientation is changing. It rather implies that the sense of rotation of the probe transition dipole is reversed periodically at the frequency of the diiodide vibration. From Figure 4 it can be seen that the anisotropy is larger when the diiodide bond is extended and smaller when the molecule

is compressed. The fact that the anisotropy increases implies that the product transition dipole is forced to turn toward the direction of the pump transition dipole whenever the diatomic fragment is extending. This behavior resembles a coupled stretch−bend motion and strongly implies that there are residual interactions between the diatomic fragment and the iodine radical. This is consistent with a time-dependent diiodide wave packet period we reported earlier.

It should be pointed out here that the anisotropy in Figure 4 exhibits a maximum value of 0.4 averaged over the vibrational coherences. This is equal to the theoretical value expected for parallel pump and probe transition dipoles and is consistent with a 530-nm probe window located in the Franck−Condon region for the pump. Furthermore, this value indicates that the modulations are not an artifact due to saturation of the optical transitions that may occur at higher excitation densities. In fact, the anisotropy at the first recurrence displays a value that is even larger than 0.4. This rather surprising result implies that the complicated motion along bending and stretching coordinates generates an orientational distribution of product transition dipoles that may not correspond to a $\cos^2 \theta$ distribution (see eq 4) as the diiodide bond is extended for the first time after bond fission in the parent molecule. This very exciting aspect of the photodissociation dynamics of triiodide is under further investigation in our laboratory.

V. Summary

In this paper, we have studied the optical anisotropy decay of diiodide ions generated through impulsive photodissociation of triiodide at 400 nm. The temporal behavior of the anisotropy is shown to involve multiple time scales, reflecting different dynamical aspects of the dissociation reaction. On ultrashort time scales well below 1 ps, the anisotropy matches the decay of the free-rotor rotational coherence. The rotational correlation times obtained from this inertial contribution give direct evidence for a significant amount of excess energy deposited into fragment rotations. This excess rotational energy is proposed to result from a broken symmetry induced by the liquid solvent environment. The geometry along the bending coordinate is estimated using an impulsive model for rotational excitation of the fragments. On picosecond time scales, the anisotropy decay is governed by diffusive reorientation of the diatomic fragment. The anharmonicity of the ground-state diiodide potential is made responsible for a pronounced wavelength dependence of the experimentally determined rotational diffusion time constant. The data also suggest strong hydrogen-bonding interactions between the diatomic product and the solvent environment. Finally, diiodide vibrational coherences have been observed in the initial decay of the transient anisotropy. This effect may be due to stretch−bend coupling of the recoiling fragments. Further experiments are currently in progress in our group that explore in more detail the dynamics of rotational energy dissipation and the early time dynamics associated with coherent product formation.

Acknowledgment. We thank Dr. D. Schwarzer for valuable discussions. We are indebted to Prof. H. Hippler and Prof. J. Troe for financial and technical support. Financial support by the Deutsche Forschungsgemeinschaft (SFB 195, "Lokalisierung von Elektronen in makroskopischen und mikroskopischen Systemen") is gratefully acknowledged.

References and Notes

(1) Schinke, R. *Photodissociation Dynamics*; Cambridge University Press: Cambridge, 1993.

(2) Zewail, A. H. *Faraday Discuss. Chem. Soc.* **1991**, *91*, 207.

(3) Banin, U.; Ruhman, S. *J. Chem. Phys.* **1993**, *98*, 4391.

(4) Banin, U.; Waldman, A.; Ruhman, S. *J. Chem. Phys.* **1992**, *96*, 2416.

(5) Zewail, A. H.; Dantus, M.; Bowman, R. M.; Mokhtari, A. *J. Photochem. Photobiol. A* **1992**, *62*, 301.

(6) Banin, U.; Kosloff, R.; Ruhman, S. *Isr. J. Chem.* **1993**, *33*.

(7) Pugliano, N.; Szarka, A. Z.; Gnanakaran, S.; Triechel, M., T.; Hochstrasser, R. M. *J. Chem. Phys.* **1995**, *103*, 6498.

(8) Pugliano, N.; Szarka, A. Z.; Hochstrasser, R. M. *J. Chem. Phys.* **1996**, *104*, 5062.

(9) Bernstein, R. B.; Zewail, A. H. *J. Chem. Phys.* **1988**, *90*, 829.

(10) Rosker, M. J.; Dantus, M.; Zewail, A. H. *J. Chem. Phys.* **1988**, *89*, 6113.

(11) Dantus, M.; Rosker, M. J.; Zewail, A. H. *J. Chem. Phys.* **1988**, *89*, 6128.

(12) Benjamin, I.; Banin, U.; Ruhman, S. *J. Chem. Phys.* **1993**, *98*, 8337.

(13) Banin, U.; Ruhman, S. *J. Chem. Phys.* **1993**, *99*, 9318.

(14) Banin, U.; Bartana, A.; Ruhman, S.; Kosloff, R. *J. Chem. Phys.* **1994**, *101*, 8461.

(15) Kühne, T.; Vöhringer, P. *J. Chem. Phys.* **1996**, *105*, 10788.

(16) Pugliano, N.; Gnanakaran, S.; Hochstrasser, R. M. *J. Photochem. Photobiol. A* **1996**, *102*, 21.

(17) Fleming, G. R. *Chemical Applications of Ultrafast Spectroscopy*; Oxford University Press: New York, 1986.

(18) Dantus, M.; Bowman, R. M.; Baskin, J. S.; Zewail, A. H. *Chem. Phys. Lett.* **1989**, *159*, 406.

(19) Baskin, J. S.; Zewail, A. H. *J. Phys. Chem.* **1994**, *98*, 3337.

(20) Wynne, K.; Hochstrasser, R. M. *Chem. Phys.* **1993**, *171*, 179.

(21) Wynne, K.; Hochstrasser, R. M. *J. Raman Spectrosc.* **1995**, *26*, 561.

(22) Berne, B. J.; Pecora, R. *Dynamic Light Scattering*; John Wiley: New York, 1976.

(23) Berne, B. J. Time-dependent properties of condensed media. In *Physical Chemistry: An Advanced Treatise*; Henderson, D., Ed.; Academic Press: New York, 1971; p 539.

(24) Berne, B. J.; Harpe, G. D. *Adv. Chem. Phys.* **1970**, *17*, 63.

(25) Gordon, G. R. *J. Chem. Phys.* **1966**, *44*, 1830.

(26) Gordon, R. G. *J. Chem. Phys.* **1965**, *43*, 1307.

(27) Gordon, R. G. *J. Chem. Phys.* **1965**, *42*, 3658.

(28) Ashkenazi, G.; Kosloff, R.; Ruhman, S.; Tal-Ezer, H. *J. Chem. Phys.* **1995**, *103*, 10005.

(29) Ashkenazi, G.; Banin, U.; Bartana, A.; Kosloff, R.; Ruhman, S. *Adv. Chem. Phys.* **1997**, *100*, 229.

(30) Gershgoren, E.; Gordon, E.; Ruhman, S. *J. Chem. Phys.* **1997**, *106*, 4806.

(31) Kühne, T.; Küster, R.; Vöhringer, P. *Chem. Phys.*, submitted.

(32) Johnson, A. E.; Myers, A. B. *J. Chem. Phys.* **1995**, *102*, 3519.

(33) Johnson, A. E.; Myers, A. B. *J. Chem. Phys.* **1996**, *104*, 2497.

(34) Johnson, A. E.; Myers, A. B. *J. Phys. Chem.* **1996**, *100*, 7778.

(35) Volk, M.; Gnanakaran, S.; Gooding, E.; Khodolenko, Y.; Pugliano, N.; Hochstrasser, R. M. *J. Phys. Chem.* **1997**, *101*, 638.

(36) Kliner, D. A. V.; Alfano, J. C.; Barbara, P. F. *J. Chem. Phys.* **1993**, *98*, 5375.

(37) Bartoli, F. J.; Litowitz, T. A. *J. Chem. Phys.* **1972**, *56*, 404.

(38) Bartoli, F. J.; Litowitz, T. A. *J. Chem. Phys.* **1972**, *56*, 413.

(39) Temkin, S. I.; Steele, W. A. *Chem. Phys. Lett.* **1993**, *215*, 285.

(40) Tasker, P. W. *Mol. Phys.* **1977**, *33*, 511.

(41) Isci, H.; Mason, W. R. *Inorg. Chem.* **1985**, *24*, 271.

(42) Okada, T.; Hata, J. *Mol. Phys.* **1981**, *43*, 1151.

(43) Chen, E. C. M.; Wentworth, W. E. *J. Phys. Chem.* **1985**, *89*, 4099.

(44) Ling, J. H.; Wilson, K. R. *J. Chem. Phys.* **1975**, *63*, 101.

(45) Levene, H. B.; Valentini, J. J. *J. Chem. Phys.* **1987**, *87*, 2594.

(46) Busch, G. E.; Wilson, K. R. *J. Chem. Phys.* **1972**, *56*, 3626.

(47) Maki, A. G.; Forneris, R. *Spectrochim. Acta* **1967**, *23*, 867. A number of rather different values for the frequency of the bending vibration can be found in the literature ranging from 52 to 85 cm^{-1}. See, for example, Gabes, W.; Gerding, H. *J. Mol. Struct.* **1972**, *14*, 267 and Mohammad, M. R.; Sherman, W. F. *J. Mol. Struct.* **1984**, *115*, 27. A value of 70 cm^{-1} seems to be a reasonable estimate for the bending frequency.

(48) Tasman, H. A.; Boswijk, K. H. *Acta Crystallogr.* **1955**, *8*, 59.

(49) Hu, C.-M.; Zwanzig, R. *J. Chem. Phys.* **1974**, *60*, 4354.

(50) Fornier de Violet, P. *Rev. Chem. Intermed.* **1981**, *4*, 121.

(51) Fleming, G. R.; Morris, J. M.; Robinson, G. W. *Chem. Phys.* **1976**, *17*, 91.

(52) von Jena, A.; Lessing, H. E. *Chem. Phys.* **1979**, *40*, 245.